Chapter 3

Numerical Studies on two-dimensional Disordered Systems in a Magnetic Field

3.1 Introduction

Periodicity of crystals allows the classification of electronic wave-functions as Bloch waves. However, in real life, the ideal crystalline state is an exception rather than the rule. Disorder exists in varying degree, ranging from a few impurities or interstitials in an otherwise perfect crystalline host to the strongly disordered limit of alloys or glasses. Recent years have seen tremendous progress in understanding disordered electronic system in their transport as well as their thermodynamic properties [1, 2]. Work has focussed both on continuum as well as discrete models. We study here a discrete model in two dimensions described by a 2d tight-binding Hamiltonian.

This chapter describes the numerical study of the single particle electronic eigenstates in disordered systems in the presence of an external magnetic field. We characterize the two types of states, localized and extended, by means of Generalized Inverse Participation Ratio (GIPR). GIPR is a quantity which measures the spatial extent of the eigenstates.

The Generalized Inverse Participation Ratio (GIPR) has been used extensively in numerical studies of metal-insulator transition[3, 4]. For a continuum disordered

model in a strong magnetic field [5, 6], this Inverse Participation Ratio (IPR) has been used to discuss various properties of disordered electronic states.

This chapter is arranged as follows. In section 2, we introduce the tight-binding Hamiltonian. We compute the density of states in section 3 and discuss its variation as we increase the strength of disorder. We use Generalized Inverse Participation Ratio as a tool to distinguish between extended and localized states in section 4. In this section, we also comment on the variation of IPR with flux. We compute GIPR for a Random Flux (RF) model. In section 5, we present a general scenario of the multi-fractal behaviour of the eigenstates in the localized regime. In this section, we comment on the general structure of GIPR exponents. In section 6. we give our conclusions.

3.2 The Tight-Binding Model

The model used in this simulation is a tight-binding model with nearest neighbour interaction and on-site random disorder. When a magnetic field is applied, the constant hopping matrix element t in the Hamiltonian is replaced by [7]

$$t_{ij} = t \ \exp\ \left(-\frac{ie}{\hbar c}\int_{r_i}^{r_j}\ d\vec{r}\cdot\vec{A}\right) \tag{3.1}$$

The 2d model Hamiltonian used here is

$$H = \sum_{<ij>}\ \left(t\ e^{2\pi ieA_{ij}}\ c_i^{\dagger}c_j + h.c.\right) + \sum_i V_i\ c_i^{\dagger}c_i \tag{3.2}$$

Here $c_i^{\dagger}$ (c_i) are the Fermionic creation (annihilation) operators with $< ij >$ referring to nearest neighbouring sites. A uniform magnetic flux per plaquette is given as $\phi = \sum_{\square}\ A_{ij} = p/q$, where the summation is over four links around a plaquette. More specifically, we apply $1/3$ flux quantum (in units of $\phi_0 = \frac{hc}{e}$) in each plaquette. We work in natural units where $\hbar = c = 1$. In all our computations we set the hopping integral t to unity. This is simply a choice of the unit of energy. Tht first term in the Hamiltonian is responsible for the band structure. The second term is the

on-site disorder one body potential generated randomly. The random numbers were generated from a uniform distribution in the interval [0,1]. We apply the periodic boundary conditions by identifying the appropriate edges of the lattice.

3.3 Density of States

In this section we discuss the density of states in the presence of disorder. We get the eigenvalues from the exact diagonalization of the model Hamiltonian for $1/3$ flux quantum per plaquette. The typical lattice size in each case is 15X15 and we also perform a disorder average of energy eigenvalues over 100 realizations. The $1/3$ flux quantum per unit cell of the lattice in this case is a commensurate flux. In figure (3.1), we show the density of states for various strengths of disorder. We start with the pure case where there is no disorder. In this case the density of states consists of three bands which is clear from figure $(3.1(a))$ and all the eigenvalues are symmetric about $E = 0$. We notice that the density of states remains statistically symmetric but about a shifted centre V/2 when we turn on a disorder potential of strength V (see figure 3.1(b) and 3.1(c)).

3.4 Inverse Participation Ratio

We arrange the energy eigenstates in the order of their energies and compute the participation ratio of the ground state. A simple analytical argument shows that the highest energy eigenstate and the ground state have the same statistical behaviour. We have checked this also numerically by computing the participation ratio of the lowest and highest energy eigenstate and verify that they are the same.

The generalized Inverse Participation Ratios are defined by the following relation

$$\mathcal{P}^r(q, L) = \left\langle \frac{\sum_i |\Psi_i^r|^{2q}}{(\sum_i |\Psi_i|^2)^q} \right\rangle \tag{3.3}$$

Here, Ψ_i^r is the i-th element of the r-th eigenstate and q is positive real number. We refer to $\mathcal{P}^r(q, L)$ as the q-th moment. $\mathcal{P}^r(2, L)$ is the usual IPR. Here, the angular

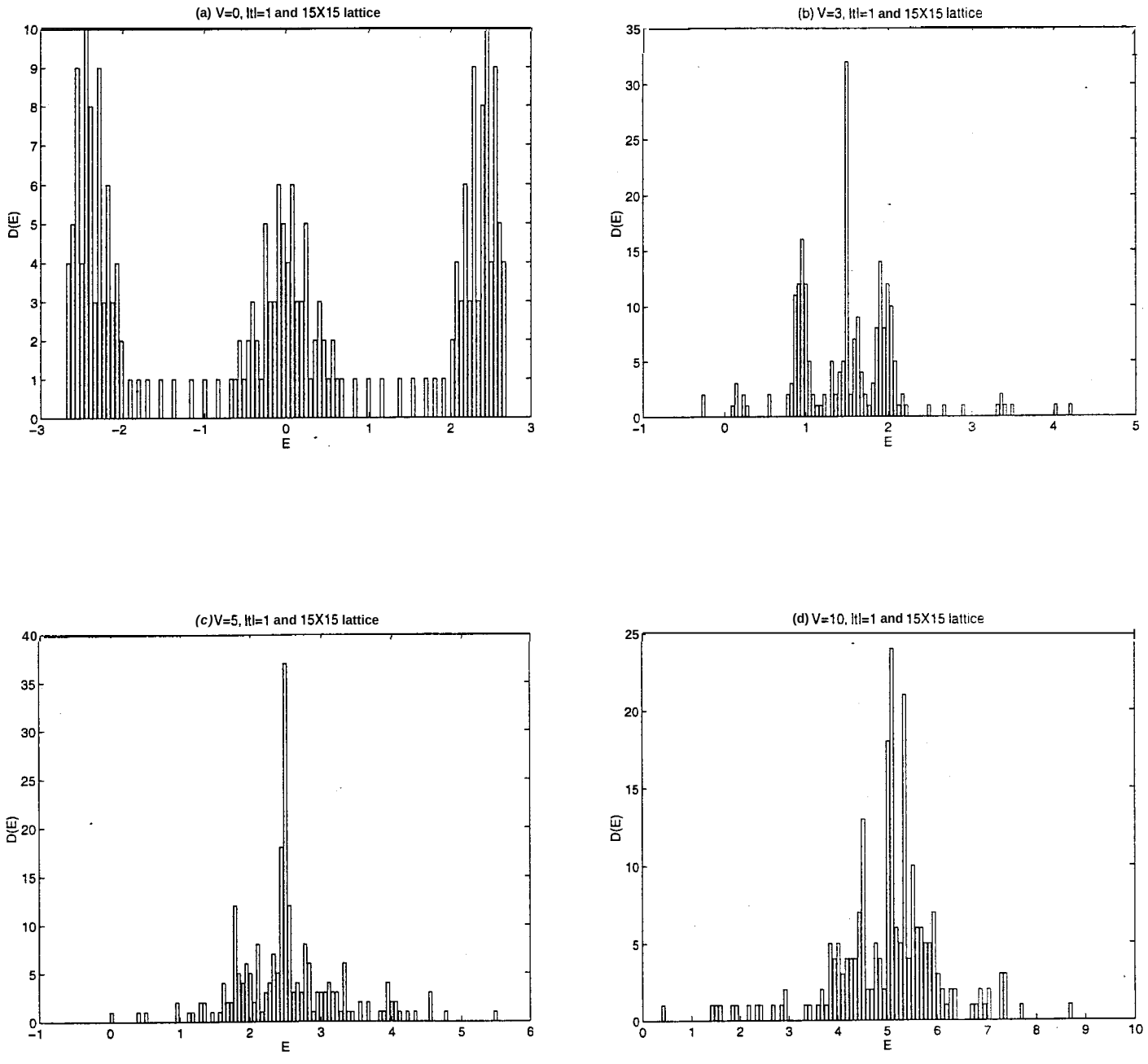

Figure *3.1: Density of states for various strengths of disorder*

bracket $\langle ... \rangle$ denotes a disorder averaging. L is the system size. We find numerically that $P^r(q, L)$ scales with L, the system size as

$$\mathcal{P}^r(q, L) \sim \frac{1}{L^{\tau(q)}} \tag{3.4}$$

The scaling exponent $\tau(q)$ is a measure of the spatial extent of the state Ψ^r. The most important participation ratio of these GIPRs is the IPR for q = 2 and this IPR is related to various fluctuations in a disordered system. Instead of $\tau(q)$, sometimes it is convenient to discuss D_q known as the generalized dimension, where D_q is related to $\tau(q)$ by $\tau(q) = (q - 1)D_q$.

We study here the relationship of $\tau(q)$ (computed from the system size dependence) with various moments in the disordered as well as in the ordered case. In figure (3.2(a)), we show a typical log-log plot of IPR (q = 2, r = 1) (the lowest state) versus the system size for two different strengths of disorder. All these data are averaged over 100 realizations of random potentials. The lattice size considered in figure (3.2(a)) is 15X15. It is evident from figure (3.2(a)) that in the disorder dominated regime IPR for V = 5 is greater than that for V = 1 for all values of the system size. Notice also in figure (3.2(a)), for V = 5 the IPR does not change appreciably after some system size L. In fact, for very large values of the system size L, it is found that the IPR remains almost constant, which characterizes a localized state.

In figure (3.2(b)), we show the variation of $\tau(q)$ vs q – 1 for two strengths of disorder. All points in this figure (3.2(b)) have been obtained through the above log-log fit (least square). Notice from the figure (3.2(b)) that for V = 1, D_q is independent of q while for V = 5, D_q does depend on q. The D_q in figure (3.2(b)) for V = 1 is .93±.02. For both cases (V = 1 and V = 5), we observe that $\tau(q)$ always increases with q. We will present later an analytical argument for this behaviour of $\tau(q)$ with q.

As we increase the strength of the disorder, the linear relationship between $\tau(q)$

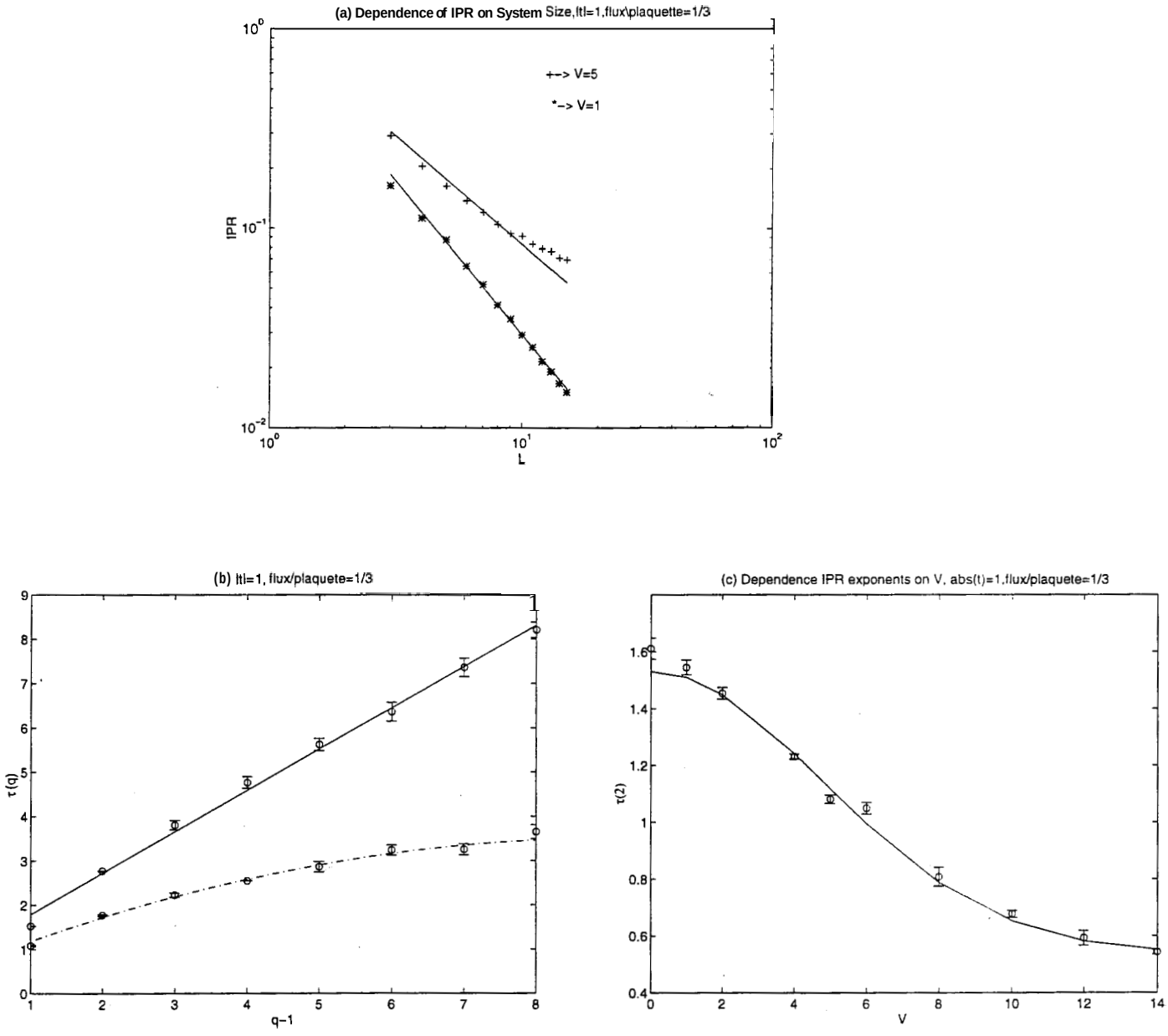

Figure 3.2: *Figure (a) represents a log-log plot of IPR with system size for two strengths of disorder potential. Figure (b) is the variation of different moments for two different strengths of disorder (solid line is for* $V = 1$ *and the other one for* V $= 5$) *and figure* (c) *is a typical uariation of the second moment with the strength of disorder. The solid line in figure (c) is a Gaussian fit given by* $\tau(2) = .9938\exp(-0.0215\ \mathrm{V}^2) + .5367$.

and q − 1 breaks down. Instead, they satisfy a non-linear relationship shown in the figure (3.2(b)). All moments of the eigenstates scale differently to give this non-linear relation. This non-linear relationship is a characteristic of a disordered system. Since, $\tau(q)$ is a non-linear function of q, the average moments cannot be described by a finite number of exponents.

In figure (3.2(c)), we depict a typical variation of the second moment exponent with the strength of the disorder. The figure shows that the IPR exponents in the localized regime are less compared to the ones in the extended regime. This can also be seen in figure (3.2(b)) explicitly for all the moments. So, the exponent for an extended state for a given moment is more than that for a localized state. With the increase in strength of disorder, the IPR exponents continuously decrease.

The solid line in figure (3.2(c)) is a Gaussian fit to the variation of the exponent with the strength of disorder. It is interesting to note that IPR exponents do not saturate to some value; instead they vanish smoothly in a Gaussian manner with the increase in disorder.

Generally, it is the centre of the band eigenstates which has been studied extensively in the literature [8]. This is of importance from the point of view of Integer Quantum Hall Effect (IQHE) [9]. However, here we have concentrated on the lowest energy eigenstate to compute the Inverse Participation Ratio. This will provide a comparison between the behaviour of the eigenstates at the centre of the band and in other positions.

3.4.1 Variation of IPR with Magnetic Flux

In this subsection, we investigate the behaviour of IPR with flux/plaquette for two different strengths of disorder. The IPR exponents were obtained for both V = 1 and V = 5 from the log-log plot of IPR with system size as discussed before. The average was taken for 100 random realizations. In this computation, the largest lattice size was taken to be 10X10 and as before, a periodic boundary condition was

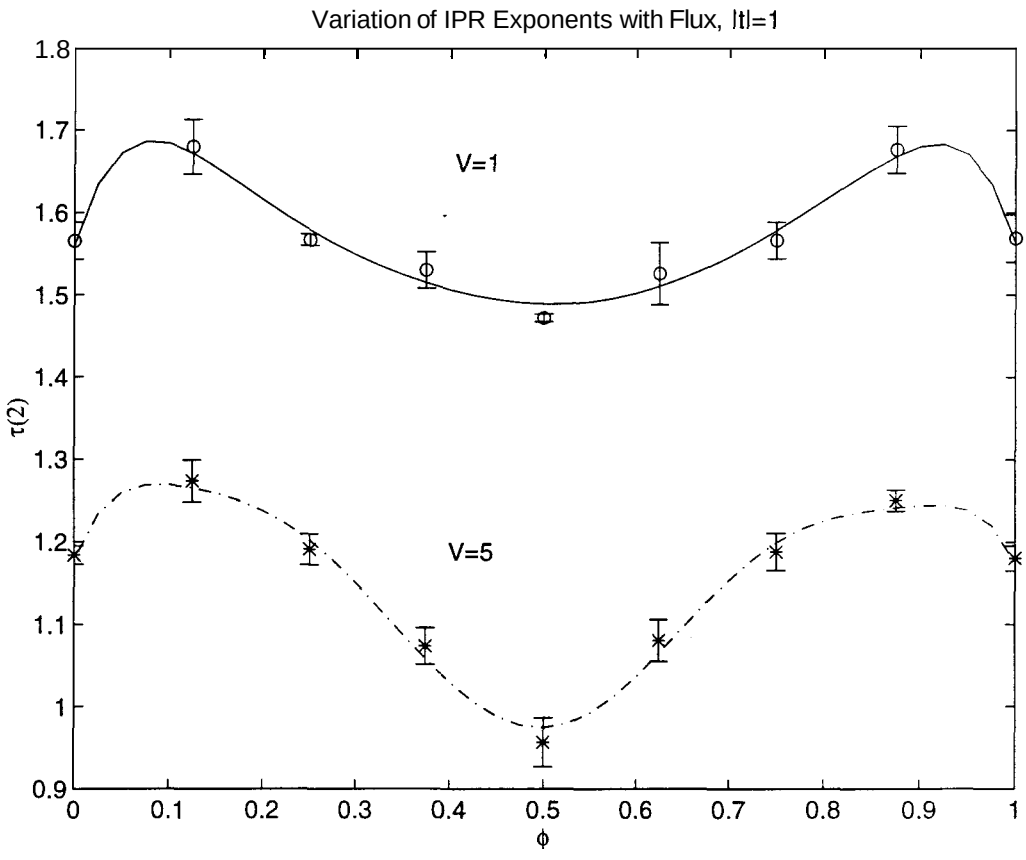

Figure **3.3:** *Variation of IPR exponents with flux/plaquette for* $V = 1$ *and* $V = 5$.

imposed. A typical variation of IPR with flux/plaquette is shown in figure **(3.3)** for $V = 1$ and $V = 5$. The first thing to notice is that the variation of IPR with ϕ for both cases is reflection symmetric about $\phi = 1/2$; $\tau(\phi) = \tau(1 - \phi)$. Secondly, for both cases IPR exponents are minimum at $\phi = 1/2$. It is also interesting to notice that for $V = 5$, the sharpness of IPR's minimum is more than that for $V = 1$. The IPR exponents for $V = 5$ are always less than that of $V = 1$ for the whole range of ϕ. We have also checked for higher moments and found the same kind of behaviour with a minimum at $\phi = 1/2$. The reflection symmetry can be understood simply. As has been mentioned before, the magnetic flux enters in the Hamiltonian in the phase of the hopping integral. This implies $\tau(\phi + 1) = \tau(\phi)$, since altering ϕ by an integer does not affect the Hamiltonian. Under time reversal the Hamiltonian for a flux ϕ $H(\phi)$ transforms to $H(-\phi)$ and the eigenstates of $H(-\phi)$ are complex conjugates of the eigenstates of $H(\phi)$. Since, the GIPR exponents depend only on $|\Psi|$, which is invariant under complex conjugation, it follows that $\tau(-\phi) = \tau(\phi)$.

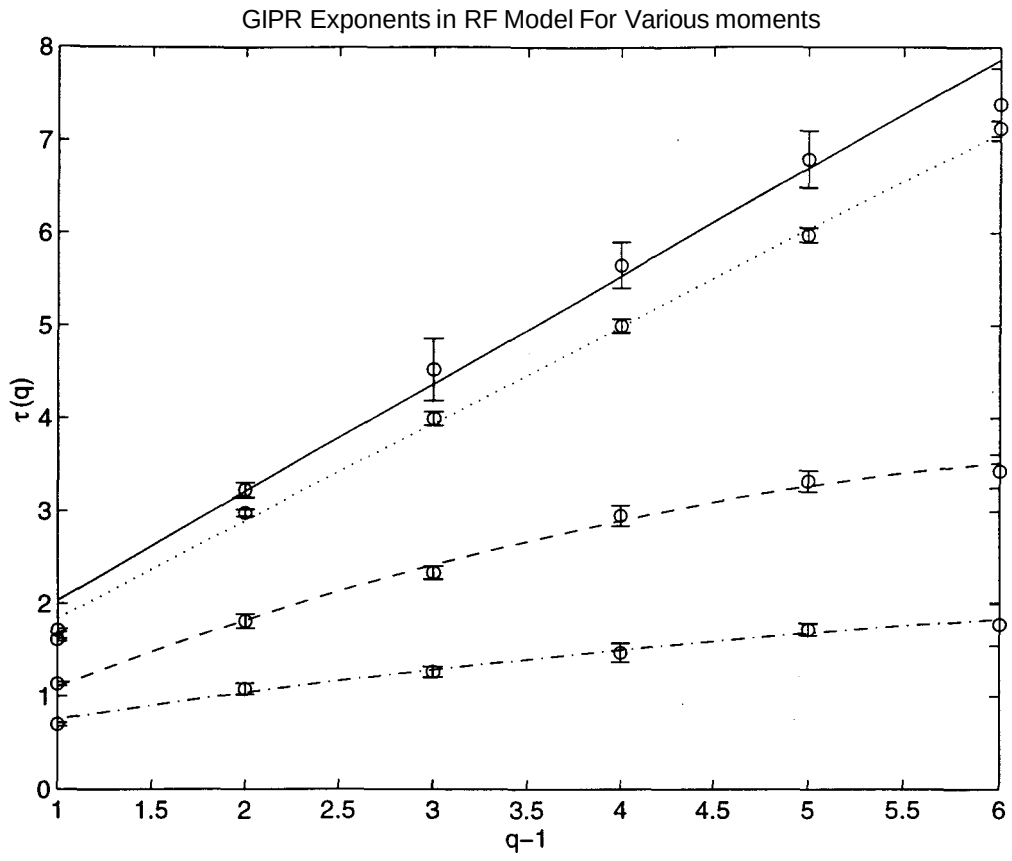

Figure 3.4: *The variation of GIPR exponents with different moments q for 4 different strength of disorder potential. The solid line, dotted line, dashed line and the dash-dotted line respectively refer to* $V = 0, 1, 5, 10$. *The bottom two lines are a quadratic fit to the data while the top two lines linear fit.*

Combining these, we get $\tau(\phi) = \tau(1 - \phi)$ which proves reflection symmetry.

3.4.2 GIPR Exponents in Random Flux Model

In this subsection, we study the various moments of the eigenstates in a Random Flux Model. Instead of a finite constant flux in the hopping element, we apply a random flux in each cell of the lattice. These random fluxes are generated from a normal distribution having mean 0 and variance 1. The on-site disorder is as before generated from a uniform distribution in the interval [0,1]. We plot in figure (3.4) $\tau(q)$ vs q $-$ 1 for 4 different sets of on-site disorder. We notice that for V $= 0$, the GIPR exponents satisfy a linear relationship among themselves. The D_qs for V $= 0$ and V $= 1$ in this random flux model are $1.05 \pm .04$ and $1.29 \pm .04$ respectively.

This should be compared with the $1/3$ flux case in figure $(3.2(\mathrm{b}))$ where we obtain for V $= 1$ case $D_q = \mathbf{.93} \pm .02$. With the increase in the strength of the disorder

potential, this linear relationship breaks dowm. This signals the appearance of localized states. The important thing to notice is that all the exponents for $V = 5$ and V = 10 are less than those of V = 0. The non-linear variation for I' = 5 and $V = 10$ can be seen explicitly if one plots them separately.

For an extended state such as a plane wave (without the magnetic field) GIPR depends on the system size L in 2-dimensions as $L^{-2(q-1)}$. This implies $\tau(q) =$ 2(q – 1). However, for an extremely disordered state such as exponential wave function, GIPR does not depend on the system size L.

An important point to notice in figure (3.2(b)) is that the slope of extended states is not equal to 2 but close to 1. In our case with 1/3 flux quantum per plaquette we find for V = 0, $\tau(2) = 1.65 \pm .01$ (and for V = 0, $\phi = 1$, $\tau(2) = 1.76 \pm .02$). This is consistent with the analytical expectation that $\tau(2) \leq 2$. Notice that $\tau(2)$ for all disorder strengths strictly obey the inequality $\tau(2) < 2$. The slope 1 of $\tau(q)$ vs q – 1 curve for the extended states in (3.2((b)) can be understootl from the following point of view. In an external magnetic field problem in 2d, we know that the motion in one direction is a plane wave while other direction is a Gaussian. From this it follows that the $\tau(q)$ is equal to q – 1 rather than 2(q – 1) for free magnetic field. To conclude this section, we notice that larger values of IPR indicate that the corresponding states are localized and smaller values of IPR indicate delocalized states.

3.5 Multifractality of Eigenstates

Multi-fractal analysis is a common tool to analyze the complexity of the disordered eigenstates [10]. The universality of multi-fractality in Quantum Hall Effect for a range of strengths of the disorder potential has been established [11].

There are two ways of determining the multi-fractal singularity spectrum. The indirect method to compute this spectrum is as follows. One computes first the

exponents of the various moments of GIPR as a function of the system size and then plots the exponents as a function of order q as has been done in figure (3.2(b)). This relation, has been denoted by $\tau(q) = (q-1)D_q$ as a function of the order q. Then, the multi-fractal spectrum is obtained through the following Legendre transform

$$f(\alpha) = q\alpha(q) - \tau(q), \qquad \alpha = \frac{d\tau}{dq} \tag{3.5}$$

Here, the function $f(\alpha)$ is to be expressed in terms of α by eliminating q from the expression for $\alpha(q)$. If $\tau(q)$ is a linear function of q (as is the case with an extended state), the above Legendre transform becomes singular.

The direct method [12, 13] takes the eigenstates explicitly for a fixed system size and then computes the $f(\alpha)$ as a function of α without going through the Legendre transform defined above. This method has also been applied in disordered mesoscopic systems [14]. To compute the multi-fractal spectrum of the eigenstates by this method, one has to define a probability distribution function as follows. We define the normalized probability distribution function as

$$P_j^r(q) = \frac{|\Psi_j^r|^q}{\sum_{k=1}^{N} |\Psi_k^r|^q} \tag{3.6}$$

where Ψ_j^r is the j-th element of r-th eigenstate.

Then, the singularity spectrum $f(\alpha)$ is defined as follows. Let

$$f(q) = \frac{-1}{\ln(N)} \sum_{j=1}^{N} P_j(q) \ln P_j(q) \tag{3.7}$$

and

$$\alpha(q) = \frac{-1}{\ln(N)} \sum_{j=1}^{N} P_j(q) \ln (|\Psi_j|), \tag{3.8}$$

where Ψ^r is normalized. Eliminating q between *(3.7)* and *(3.8)* gives $f(\alpha)$. With these definitions, it is easy to check that the function $f(q)$ satisfies the relation **(3.5).**

To compare the two methods described above for computing the multi-fractal singularity spectrum, we notice that the indirect method computes the spectrum

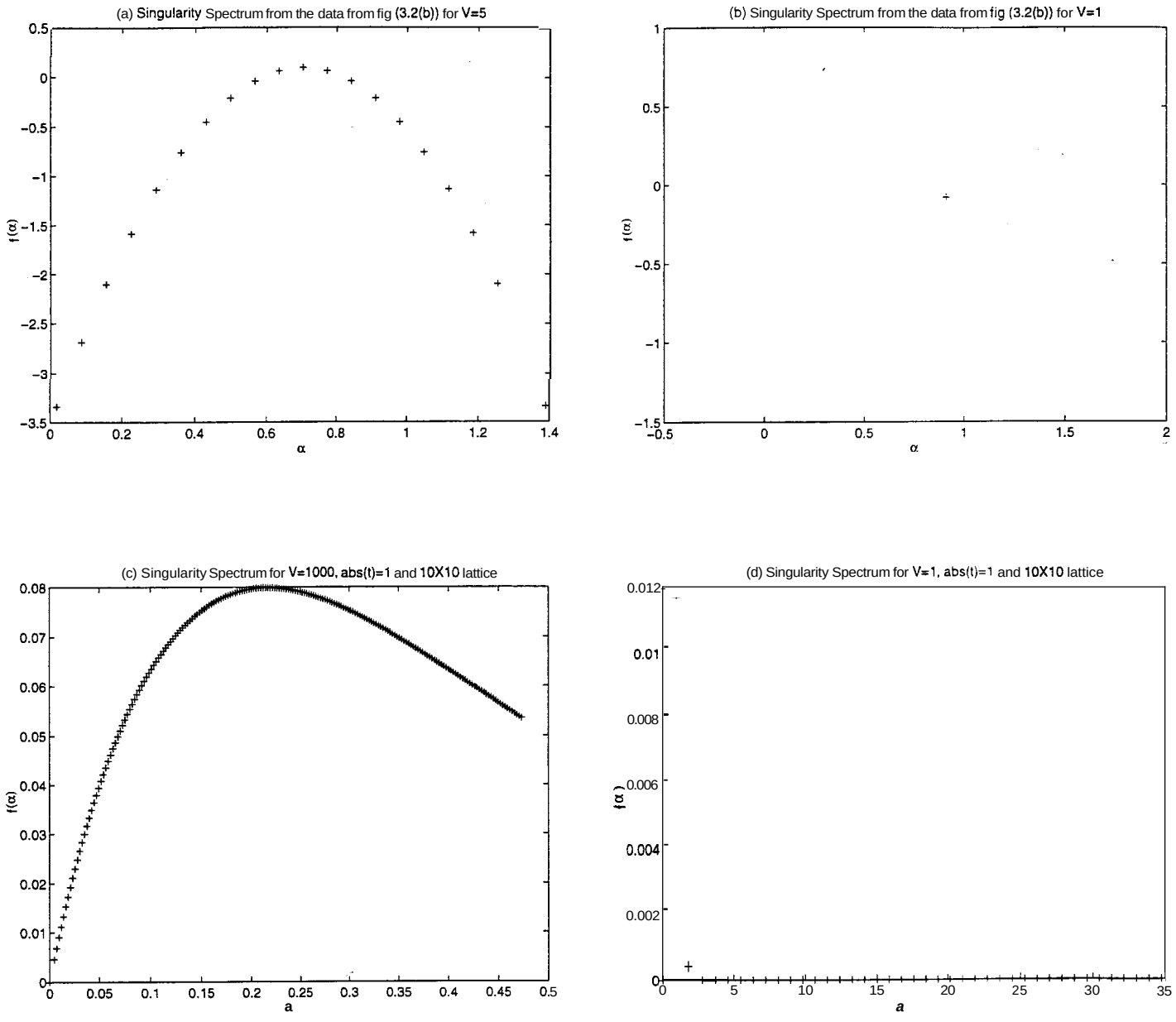

Figure **3.5:** *Multi-fractal singularity spectrum for a typical localized and extended states.*

through a Legendre transform after smoothing the $\tau(q)$ curve. This involves two steps. The error bars from the smoothing procedure make the estimation of the error bar from the data itself more difficult. Besides, if the $f(\alpha)$ or $\tau(q)$ curve exhibit any discontinuities, then this smoothing procedure usually causes one to miss some "phase transitions". The meaning of these "phase transitions" will be clear from the next section where we describe the analogy [15, 16] between multi-fractality and thermodynamics. However, in the direct method, since the multi-fractal spectrum is obtained from the eigenstates directly, no such problem arises at all.

In figure (3.5(a)) we draw the multi-fractal spectrum for $V = 5$ from the data obtained in figure (3.2(b)) through the Legendre transform defined above. The multi-fractality spectrum shown in figure (3.5(b)) was drawn directly from the figure (3.2(b)) for $V = 1$. As is clear from figure (3.5(b)), the singularity spectrum is a single point. In figure (3.5(c)) we compute the singularity spectrum directly from the eigenstates for a 10X10 lattice for a relatively strong disorder ($V = 1000$). As was mentioned in the beginning of this section, for an extended state this spectrum is a point as can be seen from the figure (3.5(d)). This is basically a consequence of the linear relationship of the IPR exponents with the moments. Another important thing to note here for the two multi-fractal spectra is that in figure (3.5(a)) the function $f(\alpha)$ starts from a negative value, then goes to a positive value crossing zero and finally becomes negative again. In contrast, in figure (3.5(c)), the function $f(a)$ always stays positive for all values of a. This behaviour is also seen for $V = 1$ in figure (3.5(b)) and (3.5(d)).

To summarize, we have shown here that the lowest energy eigenstates in the localized regime show multi-fractal behaviour. However, it is known [17] that the tail states in a disordered system do not show this multi-fractal behaviour; they have Poisson statistics. But in presence of an external magnetic field we see here their complex multi-fractal nature.

3.5.1 Relationship of Multi-fractality to Thermodynamics

In this section, we describe the connection between multi-fractality and thermodynamics [15, 16]. In a multi-fractal analysis, we compute various moments of the distribution function. We have seen earlier that for an extended state. all moments scale in the same way while for a localized state different moments scale in different way. The multi-fractal spectrum is the signature of the variation of these different moments. The distribution function can be described in terms of its moments via

$$Z_q = \sum p_i^q \tag{3.9}$$

The set of numbers $\{p_i\}$ may be used to construct a histogram $\mathcal{D}(\ln p_i)$ of "Density of States" versus $\ln(pi)$. The above equation (3.9) can be written as

$$Z_q = \sum_{\ln(p)} \mathcal{D}(\ln\ (\mathrm{p}))\, e^{-q(-\ln\ (p))} \tag{3.10}$$

Therefore, GIPR can be expressed in terms of a partition function with q playing the role of an inverse temperature β in statistical thermodynamics. The *free* energy can be defined as $F(\beta, \mathrm{L}) = -\frac{\ln Z_q}{\ln L}$. This definition easily identifies $\tau(q)$ with the free energy $F(\beta) = \lim_{L\to\infty} F(\beta, \mathrm{L})$. The above analogy with the partition function suggests that the energy E_i can be defined as $-\frac{\ln p_i}{\ln L}$. This definition allows one to identify a with the energy E $(a = \frac{\partial \tau}{\partial q} = \frac{\partial F}{\partial \beta} = \mathrm{E})$. Here, E is the average energy computed in the given distribution. In this language, entropy can be defined through the Legendre transform as $S(E, \mathrm{L}) = \beta E(\beta, \mathrm{L}) - F(\beta, \mathrm{L})$. This $S(E, \mathrm{L})$ can be traced back to $f(\mathrm{a})$.In the same spirit, one can also define the *specific* heat $C = -\frac{\partial^2 F}{\partial \beta^2} = -\frac{\partial^2 \tau}{\partial q^2}$. This completes the connection between multi-fractality and thermodynamics. To summarize, we notice

$$\begin{aligned} \beta &\leftrightarrow q, \qquad F(\beta) \leftrightarrow \tau(q) \\ E &\leftrightarrow \alpha, \qquad S(E) \leftrightarrow f(\alpha) \end{aligned} \tag{3.11}$$

At this point, we remind ourselves the fact that the "free energy" is a convex function of its arguments. This will be helpful in understanding the variation of

various parameters in the context of multi-fractality. For example, this analogy enables us to understand the shape of the $f(\alpha)$- α spectrum if one compares with the standard entropy $S(E)$ versus energy E curve in thermodynamics. The convexity of $S(E)$ allows one to understand the bell shape of the $f(\alpha)$vs α curve. One can easily see (see *3.5.2)* that $\tau(q_2) \geq \tau(q_1)$ for $q_2 > q_1$. This justifies the statement made in section **(3.4)** about the variation of GIPR exponents and is consistent with figure (3.2(b)).

To conclude, the Legendre transform $f(\alpha)$is the analog of the entropy while α is the analog of the energy E. Now, it is easy to understand the meaning of "phase transitions" in the context of the discussion in the previous section. One can simply relate the discontinuities of $f(\alpha)$or $\tau(q)$ to the discontinuities of entropy or the free energy respectively.

3.5.2 Some General Properties of $\tau(q)$

In this subsection we would like to discuss the analytic properties of $\tau(q)$ without invoking the thermodynamic analogy discussed in the previous subsection. From the definition of GIPR, we can define the probability $P_i = |\Psi_i|^2$. Since, $P_i \leq 1$, hence $\sum_i P_i^q < (\sum_i P_i)^q$ for $q \geq 0$. This immediately implies that

$$\tau(q) = -\frac{1}{\ln(L)} \ln \left(\frac{\sum_i P_i^q}{(\sum_i P_i)^q} \right) \geq 0 \tag{3.12}$$

Repeating this argument, it is easy to note that $\tau(q_2) > \tau(q_1)$ for $q_2 > q_1$. This proves that $\tau(q)$ is a monotonically increasing function of q. To prove the curvature of $\tau(q)$, we proceed as follows. We notice that

$$\alpha(q) = \frac{d\tau}{dq} = \frac{1}{\ln(L)} \left(\ln(\sum_i P_i) - \frac{Z'(q)}{Z(q)} \right) \tag{3.13}$$

where $Z(q) = \sum_i P_i^q$ and $Z'(q)$ is the derivative of $Z(q)$ with respect to q. If we impose the normalization condition on the probability, then the above equation

(3.13) turns out to be

$$\alpha(q) = -\frac{1}{\ln(L)} \left(\frac{Z'(q)}{Z(q)} \right) \tag{3.14}$$

Again the definition of $Z(q)$ implies that $Z'(q) \leq 0$ which in turn implies $\alpha(q) \geq 0$. This proves the monotonicity of $\tau(q)$ referred to in the last section. Taking one more derivative with respect to q, we find

$$\frac{d^2\tau}{dq^2} = \frac{1}{\ln(L)} \left[\frac{Z'(q)}{Z^2(q)} - \frac{Z''(q)}{Z(q)} \right] \tag{3.15}$$

This can be written from the definition of $Z(q)$ as

$$\alpha'(q) = -\frac{1}{\ln(L)} \left\langle \{\ln(P) - < \ln(P) >\}^2 \right\rangle Z^2(q) \leq 0 \tag{3.16}$$

Here, the angular bracket denotes an average over the distribution defined by $Z(q)$. Since, the variance is positive, hence the curvature of $\tau(q)$ is negative.

3.6 Conclusion

In this chapter we have studied 2d disordered systems in a magnetic field to distinguish the extended and localized states. We have separated the eigenstates by means of Inverse Participation Ratios and Multi-fractal analysis. We have also discussed the bounds on IPR for disordered eigenstates and have shown that in our discrete model the exponents do obey the bounds explicitly. The multi-fractal analysis of the eigenstates has been done by two different methods. The comparison of these two methods has been discussed. We have also provided an explanation for the variation of $\tau(q)$ with q and the shape of the f(a)-a curve.

Bibliography

[1] P. A. Lee and T. V. Ramakrishnan, Rev. Mod. Phys, 57, 287 (1985).

[2] H. Kamimura and H. Aoki, *The Physics of Interacting Electrons in Disordered Systems*, (Oxford Science Publications, Oxford, 1989).

[3] C. M. Soukoulis and E. N. Economou, Phys. Rev. Lett., 52, 565 (1984).

[4] M. Schreiber, Phys. Rev. B, **31,** 6146 (1985).

[5] B. Kramer, Y. Ono and T. Ohtsuki, Surf. Sci., 196, 127 (1988).

[6] Y. Ono, T. Ohtsuki and B. Kramer, J. Phys. Soc. Jpn., 58, 1705 (1989).

[7] R. Peierls, Z. Phys., 80, 763 (1933).

[8] D. P. Arovas, R. N. Bhatt, F. D. M. Haldane, P. B. Littlewood and R. Rammal, Phys. Rev. Lett., 60, 619 (1988); Y. Huo and R. N. Bhatt, Phys. Rev. Lett., 68, 1375 (1992); K. Yang and R. N. Bhatt, Phys. Rev. Lett., 76, 1316 (1996).

[9] R. E. Prange and S. M. Girvin eds, *The Quantum Hall Effect* (Springer-Verlag, New York, 1986).

[10] V. I. Fal'ko and K. B. Efetov, Europhys. Lett, **32,** 627 (1995).

[11] R. Klesse and M. Metzler, Europhys. Lett., **32,** 229 (1995).

[12] A. Chhabra and R. V. Jensen, Phys. Rev. Lett., **62,** 1327 (1989).

[13] T. Halsey, M. Jensen, L. Kadanoff, I. Procaccia and B. Shraiman, Phys. Rev. A, 33, 1141 (1986).

[14] W. Pook and M. Jansen, Z. Phys. B, **82,** 295 (1991).

[15] B. B. Mandelbrot, in Fluctuations and Pattern Formation, *Cargèse*, edited by H. E. Stanley and N. Ostrowsky (Kluwer, Dordrecht, 1988).

[16] M. H. Jensen, L. P. Kadanoff and I. Procaccia, Phys. Rev. A, 36, 1409 (1987).

[17] M. L. Mehta, Random Matrices, (Academic Press, London, 2nd edition, 1991).